Endosomal dysfunction contributes to cerebellar deficits in spinocerebellar ataxia type 6

Anna A. Cook[1], Tsz Chui Sophia Leung[1], Max Rice[1,2], Maya Nachman[1], Élyse Zadigue-Dubé[1], Alanna J. Watt[1*]

[1]Biology Department, McGill University, Montreal, QC, Canada.

[2]Department of Biological Sciences, Columbia University, New York, NY, USA.

[*]Correspondence: alanna.watt@mcgill.ca

Abstract

Spinocerebellar ataxia type 6 (SCA6) is a rare disease that is characterized by cerebellar dysfunction. Patients have progressive motor coordination impairment, and postmortem brain tissue reveals degeneration of cerebellar Purkinje cells and a reduced level of cerebellar brain-derived neurotrophic factor (BDNF). However, the pathophysiological changes underlying SCA6 are not fully understood. We carried out RNA sequencing of cerebellar vermis tissue in a mouse model of SCA6, which revealed widespread dysregulation of genes associated with the endo-lysosomal system. Since disruption to endosomes or lysosomes could contribute to cellular deficits, we examined the endo-lysosomal system in SCA6. We identified alterations in multiple endosomal compartments in the Purkinje cells of SCA6 mice. Early endosomes were enlarged, while the size of the late endosome compartment was reduced. We also found evidence for impaired trafficking of cargo to the lysosomes. As the proper functioning of the endo-lysosomal system is crucial for the sorting and trafficking of signaling molecules, we wondered whether these changes could contribute to previously identified deficits in signaling by BDNF and its receptor tropomyosin kinase B (TrkB) in SCA6. Indeed, we found that the enlarged early endosomes in SCA6 mice accumulated both BDNF and TrkB. Furthermore, TrkB recycling to the cell membrane in recycling endosomes was reduced, and the late endosome transport of BDNF for degradation was impaired. Therefore, mis-trafficking due to aberrant endo-lysosomal transport and function could contribute to SCA6 pathophysiology through alterations to BDNF-TrkB signaling, as well as mishandling of other signaling molecules. Deficits in early endosomes and BDNF localization were rescued by chronic administration of a TrkB agonist, 7,8-DHF, that we have previously shown restores motor coordination and cerebellar TrkB expression. The endo-lysosomal system is thus both a novel locus of pathophysiology in SCA6, and a promising therapeutic target.

Introduction

Spinocerebellar ataxia type 6 (SCA6) is an inherited ataxia which presently has no cure (Solodkin and Gomez, 2012). It is caused by a CAG expansion mutation that generates an expanded polyglutamine tract in the translated protein (Zhuchenko et al., 1997). The affected gene is *CACNA1A* (Zhuchenko et al., 1997), which encodes both the alpha subunit of voltage-gated calcium P/Q channels, as well as a putative transcription factor (Du et al., 2019, 2013). The cellular dysfunction giving rise to disease in SCA6 is poorly understood. Here we examine the role of the endo-lysosomal system in SCA6 pathophysiology.

The endo-lysosomal system comprises of a series of membrane-bound compartments that sort and transport endocytosed molecules destined for recycling or degradation (Fig. 1a) (Hu et al., 2015; Huotari and Helenius, 2011). These compartments are highly dynamic and regularly interact and fuse with each other as cargo is sorted and trafficked. Each compartment has a characteristic pH mediated by ATP-dependent acidification (Hu et al., 2015), and is characterized by the presence of specific proteins that allow them to carry out their functions. Rab GTPases regulate trafficking of cargo, and each compartment is associated with a specific signature of Rab family members (Stenmark, 2009). Endocytosed cargo arrives first at the early endosomes (Ludwig et al., 1991), where the slightly acidic pH leads to dissociation of ligands from their receptors. Here the cargo will undergo sorting: those that are destined for recycling such as receptors, will be returned to the cell surface. Cargo that is destined for further sorting or degradation will move to the late endosomes, which are characterized by an increasingly acidic pH and increased enzymatic activity (Hu et al., 2015; Huotari and Helenius, 2011). The lysosome is the final destination of cargo that is to be degraded. This compartment is the most acidic and contains over 50 hydrolases that carry out rapid degradation of cargo (de Duve, 2005; Lawrence and Zoncu, 2019).

Endosome dysfunction plays a role in the pathophysiology of several neurological diseases. A notable example is Alzheimer's disease, where postmortem brain tissue from patients displays increased early endosome size and accumulation of cargo (Cataldo et al., 2004, 2000, 1997; Tate and Mathews, 2006). Similar early endosome changes are seen in Down syndrome (Cataldo et al., 2000) and Niemann Pick C (Jin et al., 2004; Kim et al., 2023). In the cerebellum, endo-lysosomal dysfunction can lead to cerebellar dysfunction (Akizu et al., 2015; Mannan et al., 2004; Sterling et al., 2023; Vanier, 2010), and has been identified in cerebellar diseases with diverse disease-causing mechanisms (Alves et al., 2014; Zhu et al., 2022). As endosomes are the site of disassociation of ligands from their receptors, mediating both the recycling of receptors back to the cell surface and the sorting of ligands for further signaling or degradation, dysfunction can disrupt signaling pathways due to mis-trafficking of signaling molecules.

Previously, lysosomal accumulation of protein aggregates has been observed in a mouse model of SCA6 (118Q) that features a hyperexpanded polyglutamine repeat (Unno et al., 2012). This suggests that lysosomes may play a role in SCA6. Cerebellar pathology in this model was worsened when lysosomal function was impaired by the loss of the lysosomal enzyme cathepsin B (Unno et al., 2012). However, it has been unknown whether endo-lysosomal pathway dysregulation is implicated in the natural disease progression of SCA6, or whether other endosomal compartments may be involved.

We have recently found that deficits in the BDNF-TrkB-Akt signaling pathway contribute to SCA6 pathophysiology (Cook et al., 2022), with both BDNF and TrkB expression reduced in the cerebellar vermis. However, the underlying causes of the reduced levels of BDNF and TrkB remained unknown. Since both BDNF and TrkB are dynamically trafficked through the endo-lysosomal system (Moya-Alvarado et al., 2023, 2018; Yamashita and Kuruvilla, 2016), we wondered whether dysfunction in this system could underlie BDNF and/or TrkB mislocalization, contributing to subsequent cellular dysfunction in SCA6.

To address whether alterations in the endo-lysosomal system give rise to cellular dysfunction in SCA6, we examined endo-lysosomal compartments in the cerebellum of male and female $SCA6^{84Q/84Q}$ mice (referred to as SCA6 mice) in the early stages of SCA6 progression. In addition to observing abnormalities in endosomal compartments, we found that BDNF and its receptor TrkB accumulated in early endosomes instead of undergoing normal sorting and recycling. These abnormalities were present in SCA6 mice between 7 and 12 months of age, coincident with the onset of motor impairment and long before Purkinje cell degeneration (Jayabal et al., 2015). These changes therefore represent an early driver of SCA6 pathology. We were able to rescue the deficits in early endosomes with chronic administration of the TrkB agonist 7,8-DHF, a treatment that we previously found could also rescue behavioural and Purkinje cell firing deficits in the SCA6 mice. Our findings argue that endo-lysosomal dysfunction is a novel locus of pathophysiology in spinocerebellar ataxia and a potential therapeutic target to investigate further.

Results

The endo-lysosomal system (Fig. 1a) is critical for proper cellular function and its dysregulation is associated with mis-trafficking of important cargo. Here we address whether endo-lysosomal dysfunction contributes to SCA6, using a mouse model ($SCA6^{84Q/84Q}$ mice, referred to as SCA6 mice) that robustly models the mid-life onset of motor deficits and cerebellar dysfunction seen in SCA6 patients (Jayabal et al., 2015; Watase et al., 2008). We have previously shown that around 7 months of age, SCA6 mice develop deficits in motor coordination that progressively worsen (Jayabal et al., 2015, 2016) and display cellular deficits, including aberrant Purkinje cell firing and disrupted BDNF-TrkB signaling (Chang et al., 2022; Jayabal et al., 2016). But the cellular alterations that lead to the reduction of BDNF and TrkB in the SCA6 cerebellum remained unknown, so we conducted further investigation into potential causes.

We carried out RNA sequencing on cerebellar vermis tissue from 12-month-old litter-matched wildtype (WT) and SCA6 mice (N=5 for each genotype) during the course of another investigation. This sequencing revealed that many genes involved in the endo-lysosomal system, as defined by the gene ontology (GO:CC) terms "Endosome" (GO:0005768) and "Lysosome" (GO:0005764), were significantly dysregulated in the SCA6 cerebellum (Fig. 1b, Padj < 0.05, see Supplementary Table 1 for a full list). The expression levels of these genes were altered by between 10% and 200% in SCA6 compared to WT. Endosomal genes were found to be both up- and down-regulated in SCA6, but the genes covered by the Lysosome GO term were mostly upregulated compared to WT. The affected genes are associated with multiple endosomal compartments, meaning that the cellular consequences could be wide reaching. We therefore aimed to determine whether different compartments of the endo-lysosomal system (Fig. 1a) are altered in the cerebellum of SCA6 mice, and whether this could contribute to previously described BDNF and TrkB deficits, via mis-trafficking through the endo-lysosomal system.

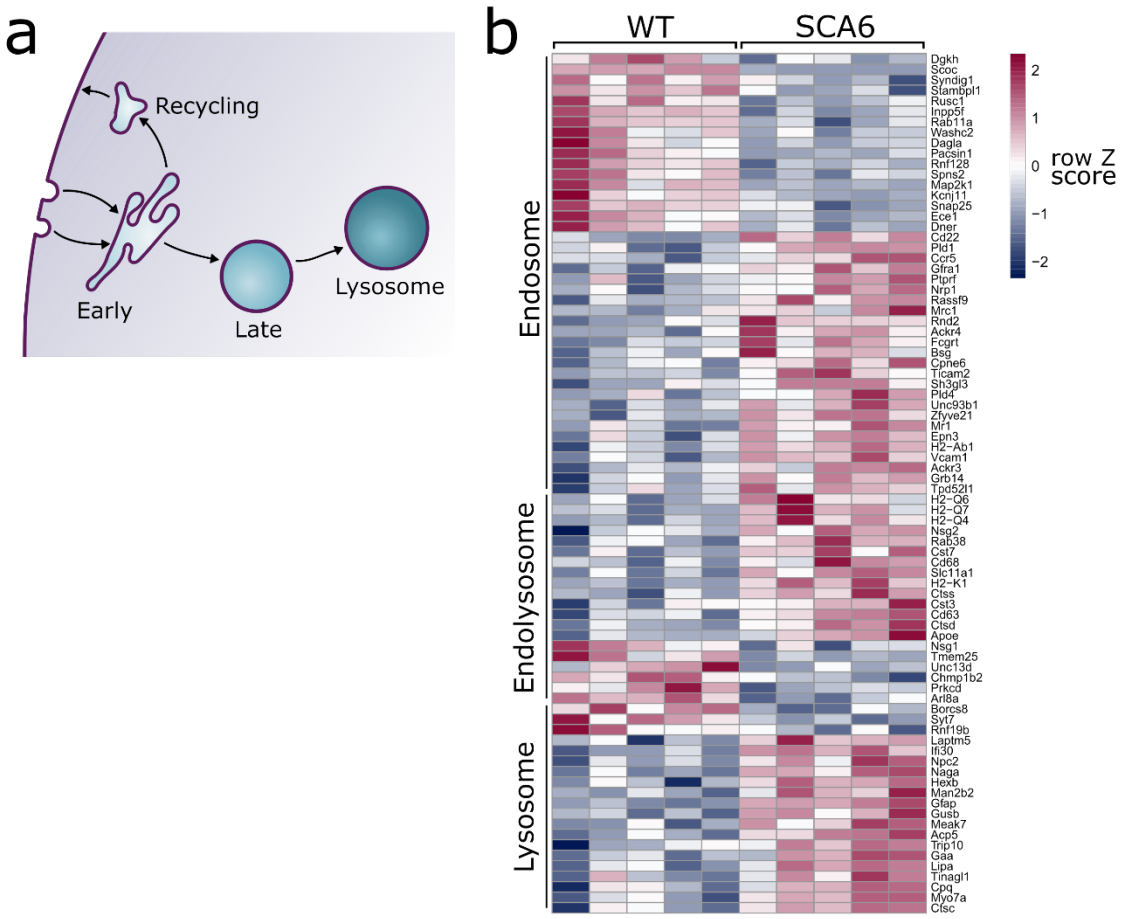

Figure 1: Endo-lysosomal genes are dysregulated in the SCA6 cerebellum.
(a) Schematic showing the endo-lysosomal system. (b) Heat map showing relative expression of endo-lysosomal associated transcripts in the cerebellum of 5 WT and 5 SCA6 mice (1 column per mouse). Genes are separated into groups based on their gene ontology categorization (GO term Endosome and Lysosome; the group "Endolysosome" denotes genes that belong to both GO term categories), only genes with an adjusted P value < 0.05 are shown.

Early endosomes are enlarged and accumulate BDNF and TrkB in Purkinje cells in SCA6 mice.

Early endosomes are the first stop for newly endocytosed cargo. There, cargo undergoes sorting as the slightly acidic pH facilitates ligand release from receptors (Fig. 2a). We carried out immunohistochemistry (IHC) against early endosome antigen 1 (EEA1) on sections of cerebellar vermis from 7–8-month WT and SCA6 mice and found that EEA1 staining is present in the cerebellum, particularly in Purkinje cells (Fig. 2b). We imaged Purkinje cells and could identify large tubular early endosomes in Purkinje cell somas of both WT and SCA6 mice (Fig. 2b, c). The early endosome marker in SCA6 Purkinje cells covered a larger area, showing that the early endosome compartment is enlarged in SCA6 (Fig. 2d). A similar enlargement of early endosomes has been seen in other neurological diseases (Cataldo et al., 2000, 1997; Jin et al., 2004). Using the EEA1 marker to delineate early endosomes, we were able to analyze BDNF and TrkB localized within the early endosome compartment. There was a higher amount of BDNF staining within the early endosomes of Purkinje cells from SCA6 mice (Fig. 2e, f). This was intriguing as we have previously shown that BDNF levels in the cerebellar vermis as a whole are decreased (Cook et al., 2022), so BDNF accumulates specifically in this compartment despite depressed levels overall in the cerebellum. We found the same was true for TrkB, as TrkB immunoreactivity was increased within the EEA1 positive early endosome compartment in SCA6 Purkinje cells compared to WT (Fig. 2g, h). Nearly all of the TrkB staining within SCA6 Purkinje cells colocalized with the EEA1 marker (Fig. 2g, arrowheads), whereas the tissue from WT mice showed abundant TrkB staining outside the early endosome compartment of Purkinje cells (Fig. 2g, arrowheads). Thus, early endosomes are enlarged and accumulate BDNF and TrkB in SCA6, despite decreased levels of both proteins in the SCA6 cerebellum as a whole. This cargo mis-trafficking could lead to a decrease in the amount of free BDNF available to signal, as well as the amount of TrkB recycled to the cell surface, thereby contributing to previously described BDNF-TrkB signaling deficits in SCA6 (Cook et al., 2022).

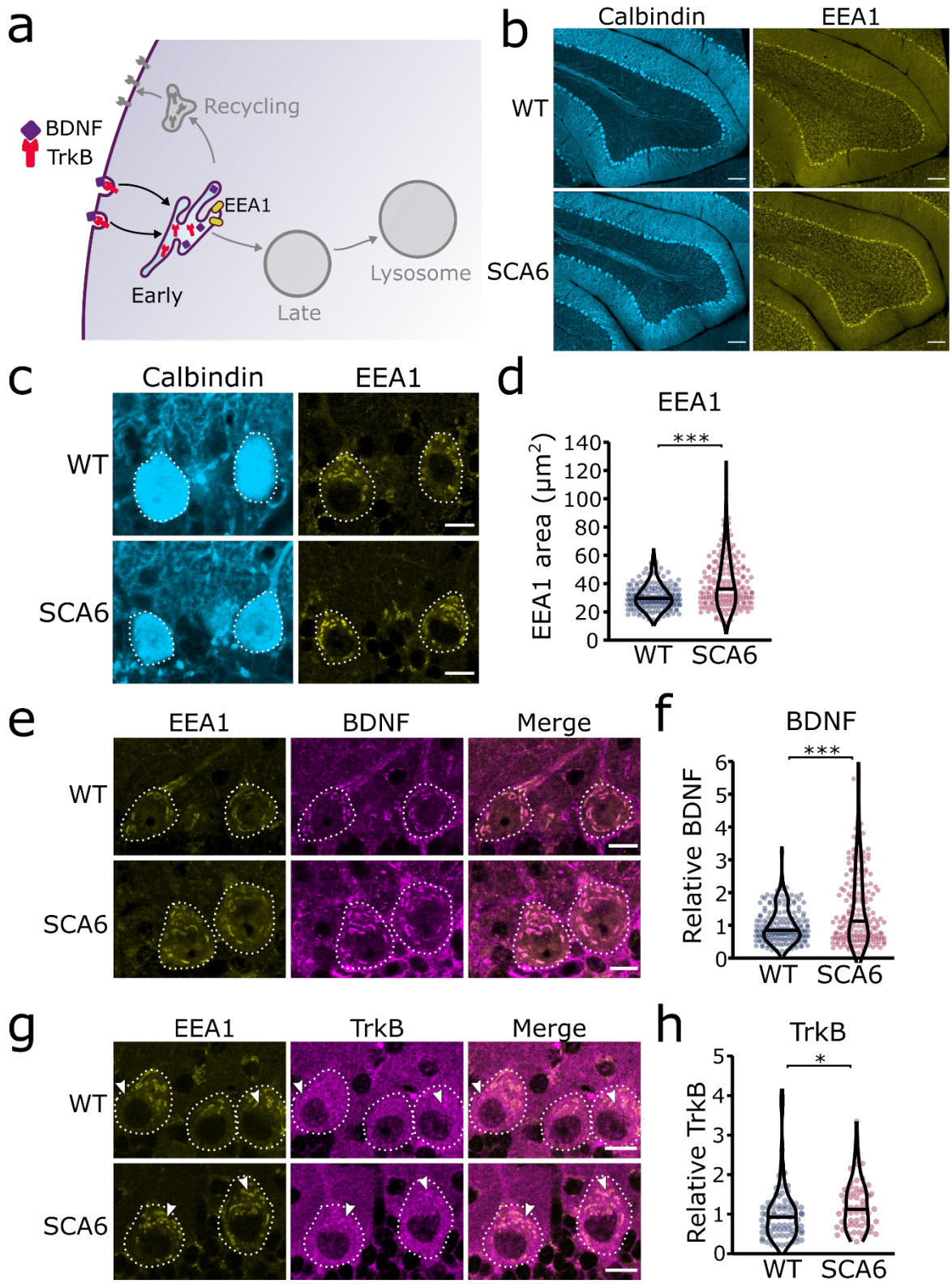

Figure 2: Early endosomes are enlarged and accumulate BDNF and TrkB in SCA6 Purkinje cells. (a) Schematic showing BDNF and TrkB endocytosis and trafficking to early endosomes labeled with EEA1. (b) The early endosome marker EEA1 stains early endosomes in lobule 3 of the cerebellar vermis in WT

143 and SCA6 mice, calbindin labels Purkinje cells. Scale bar, 100µm. (c) Closeup images of the early
144 endosome marker EEA1 in lobule 3 of cerebellum, calbindin labels Purkinje cells (outlined). Scale bar,
145 10µm. (d) The area covered by EEA1 staining in Purkinje cells is increased in SCA6 mice compared to WT
146 ($P < 0.001$; N = 6 WT mice, 173 cells; 5 SCA6 mice, 171 cells). (e) Representative images of the early
147 endosome marker EEA1 and BDNF within Purkinje cells (outlined) in the anterior vermis. Scale bar, 10µm.
148 (f) Relative staining level of BDNF within early endosome compartment is higher in the Purkinje cells of
149 SCA6 mice compared to WT ($P < 0.001$; N = 6 WT mice, 173 cells; 5 SCA6 mice, 171 cells). (g)
150 Representative images of the early endosome marker EEA1 and TrkB within Purkinje cells (outlined) in
151 the anterior vermis. Arrowheads denote locations of significant TrkB accumulations. Scale bar, 10µm. (h)
152 Relative staining level of TrkB within early endosome compartment is higher in the Purkinje cells of SCA6
153 mice compared to WT ($P = 0.013$; N = 4 WT mice, 79 cells; 4 SCA6 mice, 58 cells). Mann Whitney *U* test
154 used for all statistical comparisons, * $P < 0.05$, *** $P < 0.001$.
155
156 **Recycling endosomes are morphologically normal in SCA6.**
157 Since we identified an accumulation of TrkB in early endosomes, we wondered whether this would affect
158 the amount of TrkB recycled back to the cell surface. Recycling endosomes return receptors to the plasma
159 membrane for further signaling (Fig. 3a) (O'Sullivan and Lindsay, 2020). Syntaxin 12/13 involved in
160 recycling of endocytosed proteins back to the plasma membrane and is located in recycling endosomes and
161 some tubular protrusions from early endosomes that are also involved in recycling (Prekeris et al., 1998).
162 We used two different antibodies for Syntaxin 12/13 (Stx13) as a marker for recycling endosomes. Staining
163 with both antibodies revealed a large network of small recycling endosomes in Purkinje cells (Fig. 3b, Supp.
164 Fig 1). Analysis revealed that recycling endosome area was unchanged in SCA6 Purkinje cells (Fig. 3c,
165 Supp. Fig. 1). We noted colocalization between TrkB and Stx13, showing TrkB being recycled back to the
166 cell surface after dissociation from bound BDNF in the early endosomes. The TrkB staining within the
167 recycling endosome compartment marked by Stx13 was decreased in Purkinje cells in SCA6 mice (Fig.
168 3d). Combined with the increased levels of TrkB in the early endosomes of Purkinje cells in SCA6 (Fig.
169 2h), these data argue that TrkB is stuck in early endosomes in SCA6, rather than being recycled to the cell
170 surface to the same extent as in WT Purkinje cells. This mislocalization may contribute to the depressed
171 levels of BDNF-TrkB signaling previously described in SCA6 (Cook et al., 2022).

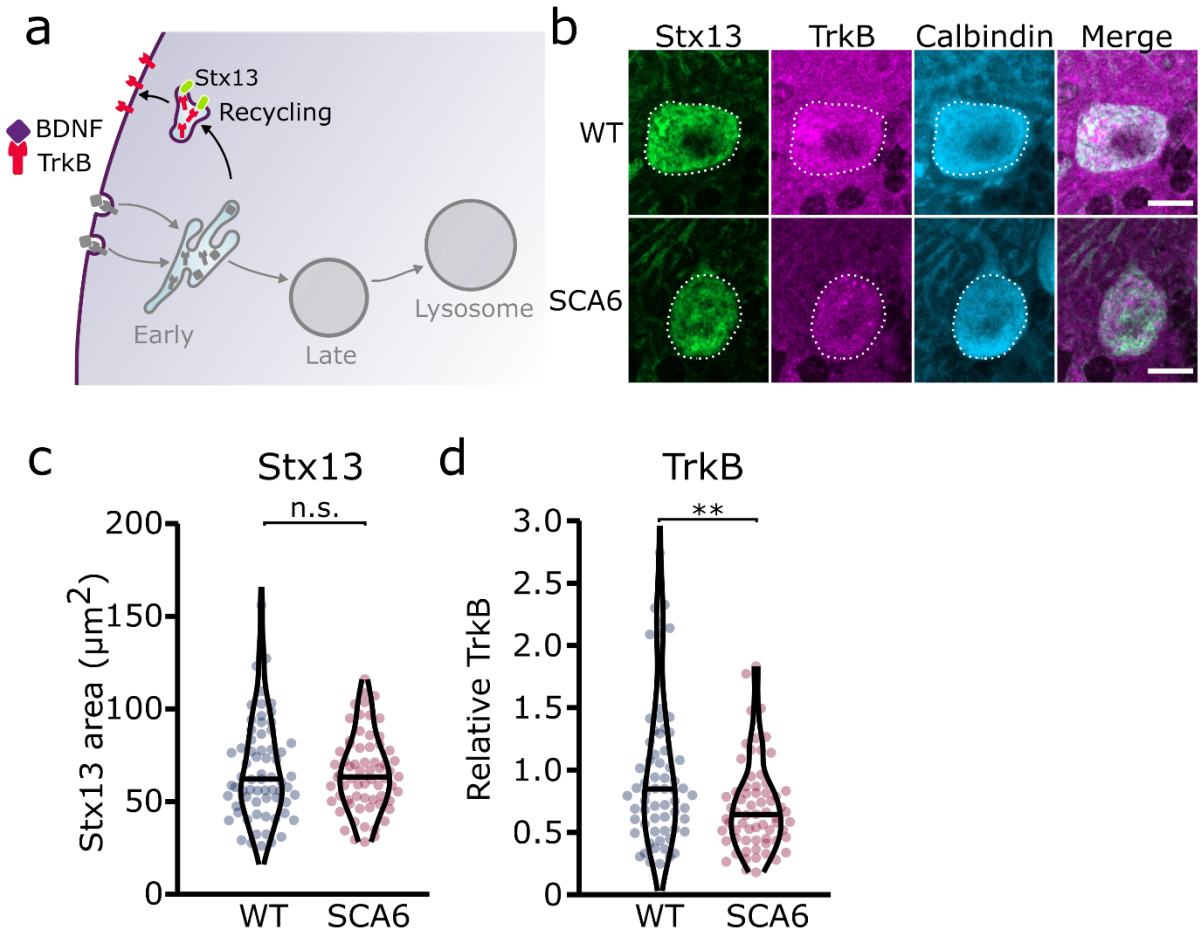

Figure 3: Recycling of TrkB in recycling endosomes is impaired in SCA6 Purkinje cells. (a) Schematic showing the return of TrkB to the cell membrane via recycling endosomes labeled with Stx13. (b) Representative images of the recycling endosome marker Stx13 and TrkB within Purkinje cells (outlined) of the anterior vermis. Scale bar, 10μm. (c) The area covered by Stx13 staining in Purkinje cells is unchanged between WT and SCA6 mice ($P = 0.96$; N = 4 WT mice, 67 cells; 4 SCA6 mice, 66 cells). (d) The relative level of TrkB within recycling endosomes was significantly decreased in SCA6 Purkinje cells ($P = 0.0034$; N = 4 WT mice, 67 cells; 4 SCA6 mice, 66 cells). Mann Whitney *U* test used for all statistical comparisons, ** $P < 0.01$, n.s. $P > 0.05$.

Late endosomes

Early endosomes undergo maturation into late endosomes in order to transport cargo destined for degradation to the lysosomes (Huotari and Helenius, 2011) (Fig. 4a). Neurons use this degradative pathway as a way to regulate BDNF levels (Evans et al., 2011). We used Rab7 as a marker for late endosomes (Vitelli et al., 1997), and identified numerous late endosomes in Purkinje cells of both WT and SCA6 mice (Fig. 4b). The Rab7 staining covered a smaller area in the Purkinje cells of SCA6 mice compared to WT (Fig. 4c), indicating a reduction in the size or number of late endosomes. Most of the BDNF staining within the Purkinje cells did not colocalize with Rab7 (Fig. 4b), which was expected as we had previously found high levels of colocalization of BDNF with the early endosome marker EEA1 (Fig. 2e). The BDNF staining that was present within the Rab7 positive late endosome compartment was significantly reduced in SCA6 compared to WT (Fig. 4d), suggesting that BDNF accumulates in the early endosomes earlier in the

endosomal pathway (Fig. 2f), preventing its progression through the late endosomal stage. Late endosomes transport cargo to lysosomes for degradation, so less BDNF may reach the lysosome in SCA6. This could have implications for the regulation of BDNF within Purkinje cells, as neurons tightly regulate BDNF levels via degradative pathways (Evans et al., 2011).

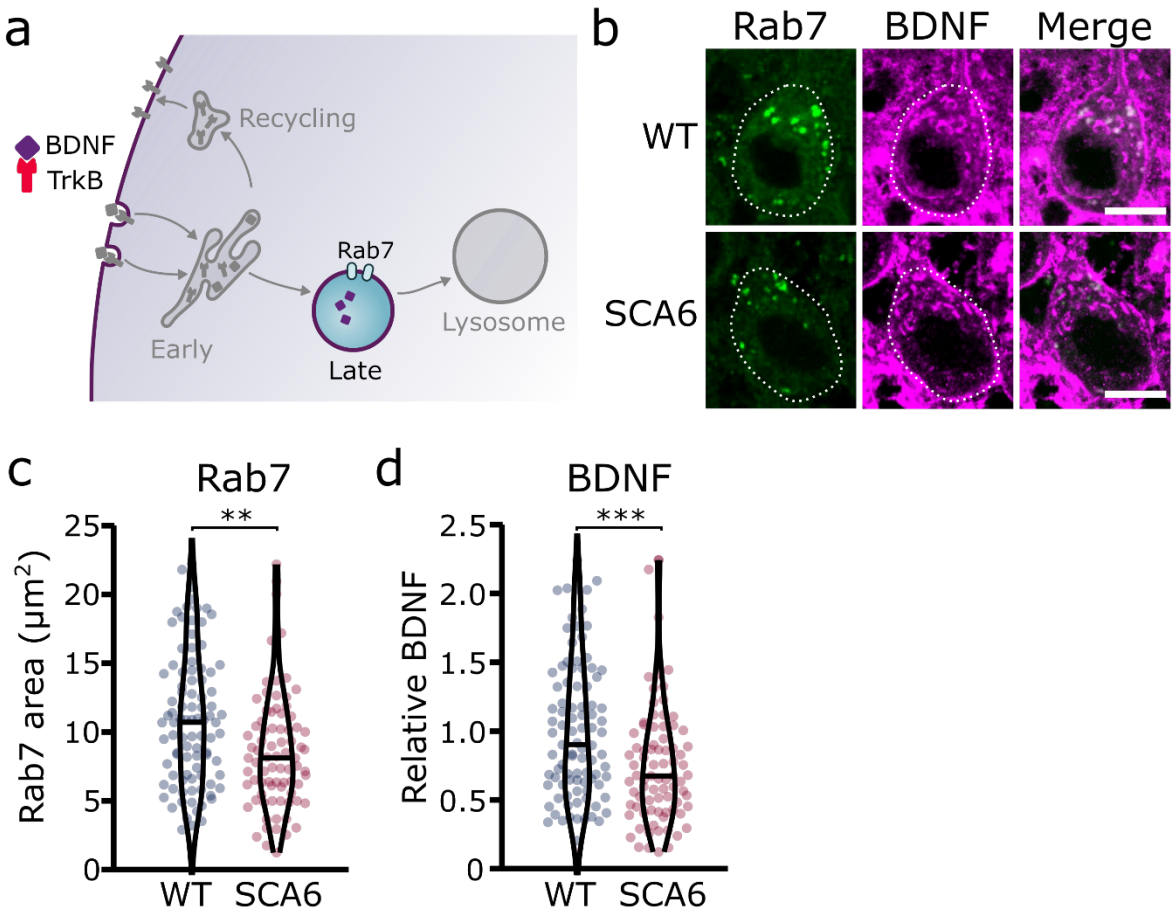

Figure 4: Late endosomes are reduced in SCA6 Purkinje cells and carry less BDNF.
(a) Schematic showing the transport of BDNF in late endosomes expressing Rab7. (b) Representative images of the late endosome marker Rab7 and BDNF within Purkinje cells (outlined) of the anterior vermis. Scale bar, 10μm. (c) The area covered by Rab7 staining in Purkinje cells is decreased in SCA6 mice compared to WT ($P = 0.0019$; N = 4 WT mice, 93 cells; 4 SCA6 mice, 81 cells). (d) The relative level of BDNF within late endosomes was significantly decreased in SCA6 Purkinje cells ($P < 0.001$; N = 4 WT mice, 93 cells; 4 SCA6 mice, 81 cells). Mann Whitney *U* test used for all statistical comparisons, ** $P < 0.01$, *** $P < 0.001$.

Lysosomal morphology is unchanged in SCA6.
We next aimed to determine whether lysosomes were altered in SCA6, using a dual strategy to visualize the lysosomes in cerebellar slices. We first used a pH sensitive dye, LysoTracker Red DND 99, to visualize the acidic lysosomes (Fig, 5a, b) (Chazotte, 2011). As LysoTracker labels all acidic compartments, it is not sufficient to confirm the identity of lysosomes. This may be particularly problematic if other intracellular compartments undergo inappropriate acidification, which has been observed in other neurological diseases (Pescosolido et al., 2021). Therefore, after staining acute cerebellar slices with LysoTracker, we performed immunohistochemistry for Lysosomal-associated membrane protein 1 (Lamp1), a glycoprotein localized at

215 the membranes of lysosomes. Because even Lamp1 can be localized outside of lysosomes (Cheng et al.,
216 2018), we used both LysoTracker and Lamp1 to identify lysosomes in Purkinje cells. We found that both
217 stains labelled lysosomes within Purkinje cells (Fig. 5b). As expected, the Lamp1 staining appeared as ring
218 like structures, marking the membranes of the lysosomes, while LysoTracker staining marked the acidic
219 lumen of the lysosomes, in the center of these rings (Fig. 5b, see zoom). While Lamp1 staining identified a
220 large number of lysosomes of varying size, the LysoTracker stain was present only in the largest. This
221 discrepancy has been noted previously, as LysoTracker does not label the smallest lysosomes in cerebellar
222 slices or other cell preparations that are fixed after staining (Chazotte, 2011; Song et al., 2008). We found
223 that the total area covered by the Lamp1 and LysoTracker stains was not significantly different between
224 Purkinje cells from WT and SCA6 mice (Fig. 5c, d). The area of colocalization between the two stains was
225 also unchanged (Fig. 5e).
226
227 To investigate further and determine whether the two stains label the same population of lysosomes in the
228 two genotypes, we counted the number of lysosomes labelled by different combinations of the two markers.
229 The lysosomes labelled by these two strategies could be divided into 3 groups. (1) Compartments stained
230 by both Lamp1 and LysoTracker, confirming that they are indeed lysosomes. The number of these
231 lysosomes was indistinguishable between WT and SCA6 mice (Fig. 5f), indicating that Lamp1 positive
232 lysosomes are present in normal quantities and are appropriately acidified in SCA6 Purkinje cells. In
233 agreement, the area covered by each stain per lysosome, a proxy for the size of the lysosomes, was
234 unchanged in SCA6 (Supp. Fig. 2). (2) Lysosomes labelled by Lamp1 but not LysoTracker (Fig. 5g)
235 represent small lysosomes unable to retain the LysoTracker dye after fixation (Chazotte, 2011; Song et al.,
236 2008). This number was not significantly different between WT and SCA6 mice and so Lamp1 appears to
237 be present at normal levels and is appropriately localized to lysosomes in SCA6. (3) Organelles labelled by
238 LysoTracker but not Lamp1 could include maturing late endosomes or other endosomal compartments that
239 are inappropriately acidified. Late endosomes have an acidic pH and Rab7 positive late endosomes can be
240 LysoTracker positive (Majzoub et al., 2016). Late endosomes fuse with lysosomes to complete cargo
241 degradation, but first they mature into an intermediate compartment called an endolysosome (Huotari and
242 Helenius, 2011). Therefore, these LysoTracker-positive Lamp1-negative organelles could be late
243 endosomes or intermediate endolysosomes that have not yet fused with the Lamp1 positive lysosomes. The
244 number of these compartments was low in Purkinje cells in both genotypes but was significantly lower in
245 SCA6 mice (Fig. 5h). This agrees with our finding of a reduction in the size of the late endosome
246 compartment in SCA6 mice (Fig. 4c). A reduction in the late endosome compartment suggests that there
247 are fewer late endosomes available to mature and fuse with lysosomes. Therefore, the Lamp1 positive
248 lysosomes are morphologically normal in the Purkinje cells of SCA6 mice while the small alteration in
249 Lysotracker staining likely represents a deficit in the maturation of late endosomes before fusion with
250 lysosomes.

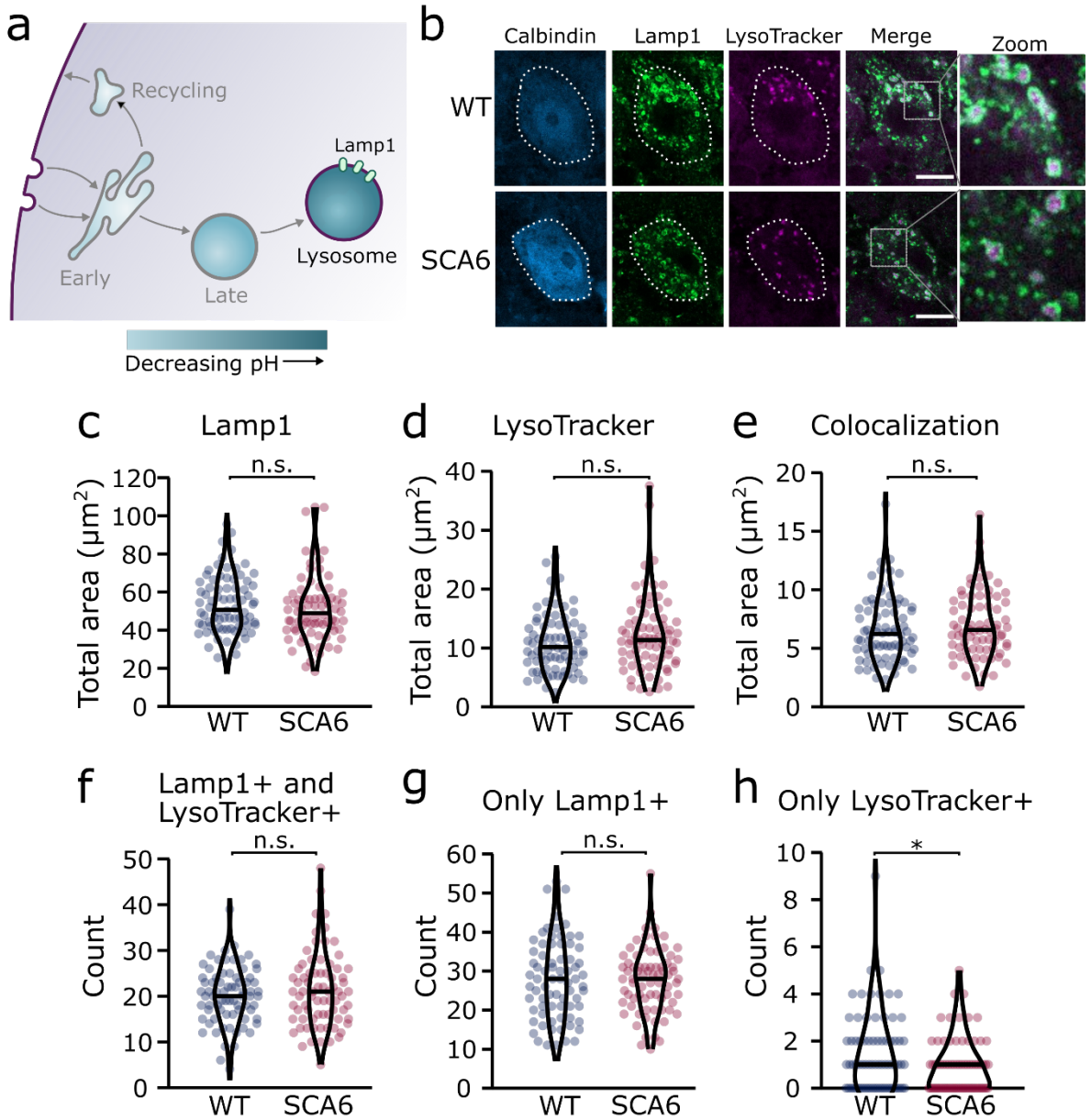

Figure 5: Lysosomes in SCA6 Purkinje cells are morphologically normal but there may be a deficit in late endosome maturation.

(a) Schematic showing the endo-lysosomal system as a series of compartments of increasingly acidic pH with lysosomes, expressing Lamp1, being most acidic. (b) Representative images of Purkinje cells in the anterior vermis stained for the lysosome membrane marker Lamp1 and LysoTracker as a marker of acidic compartments. Calbindin labels Purkinje cells (outlined). Scale bar, 10µm. The area covered by (c) Lamp1 staining and (d) LysoTracker staining in Purkinje cells is unchanged between WT and SCA6 mice (P = 0.26 for Lamp1; P = 0.20 for LysoTracker; N = 3 WT mice, 78 cells; 3 SCA6 mice, 76 cells). (e) The area of colocalization between Lamp1 and Lysotracker is unchanged between WT and SCA6 mice (P = 0.34; N = 3 WT mice, 78 cells; 3 SCA6 mice, 76 cells). (f) The number of lysosomes that were both Lamp1 positive and LysoTracker positive was not significantly different between genotypes (P = 0.72; N = 3 WT mice, 78 cells; 3 SCA6 mice, 76 cells). (g) The number of lysosomes that were Lamp1 positive, but LysoTracker

negative was unchanged between genotypes (P = 0.83; N = 3 WT mice, 78 cells; 3 SCA6 mice, 76 cells). (h) The number of putative late endosomes undergoing maturation that were Lamp1 negative, but LysoTracker positive was significantly decreased in the Purkinje cells of SCA6 mice (P = 0.034; N = 3 WT mice, 78 cells; 3 SCA6 mice, 76 cells). Mann Whitney *U* test used for all statistical comparisons except number of Lamp1+ puncta (f) which was normally distributed and so a Student's *t* test was used, * P < 0.05, n.s. P > 0.05.

Taken together, these results suggest that although lysosomes are present in normal numbers, the trafficking of endocytosed cargo to the lysosome for degradation is impaired in the SCA6 cerebellum. Our transcriptomic data furthermore shows that genes encoding lysosomal proteins are abnormally expressed in SCA6 (Fig. 1b), suggesting that lysosomal dysfunction is present in SCA6. Lysosomes are enzymatically active sites of degradation and contain multiple proteases that rapidly break down proteins. However, lysosomal proteolysis depends not just on enzymatic activity, but on the correct transport of proteins to the lysosomes through endosomal compartments. We wondered whether the deficits we identified in early and late endosomes (Fig. 2, 4), or other deficits in lysosome activity, might impair the ability of lysosomes to degrade endocytosed cargo in SCA6. We assayed this by incubating acute cerebellar slices with BODIPY FL Pepstatin A, an exogenous peptide that can be endocytosed and transported to the lysosome, where it binds to the active form of the lysosomal enzyme Cathepsin D (Chen et al., 2000) (Fig. 6a). We could visualize Pepstatin A signal within Lamp1 positive puncta, demonstrating Cathepsin D enzymatic activity within lysosomes (Fig. 6b). The Pepstatin A signal within Purkinje cells was significantly reduced in SCA6 mice (Fig. 6c, d), revealing a lower level of either the endocytosed construct, or of active Cathepsin D. The identification of alterations in the early and late endosomes that transport cargo to the lysosomes (Fig. 2, 4), suggests that SCA6 Purkinje cells have endosomal deficits that reduce transport of the endocytosed Pepstatin A construct to the lysosome where it can bind active Cathepsin D. This finding is therefore consistent with an overall impairment of endo-lysosomal trafficking. The reduction in Pepstatin A signal would also be consistent with a reduction in Cathepsin D enzymatic activity that could further contribute to aberrant handling of endocytosed cargo in SCA6. RNA-sequencing identified an upregulation of lysosomal enzyme transcripts in the SCA6 cerebellum, including the *CTSD* gene encoding Cathepsin D (Fig. 1b). However, this would not necessarily lead to an increase in enzyme activity as the RNA must first be translated, and then undergo post-translational proteolytic processing in order to produce the active form of Cathepsin D that binds Pepstatin A (Zaidi et al., 2008). This suggests that in SCA6, there is an upregulation in *CTSD* and other lysosomal genes that does not lead to an increase in functional enzymes. This may be a compensatory mechanism for trafficking deficits of cargoes to the lysosomal compartment, or an attempt to compensate for deficits in the production of the active form of Cathepsin D. In summary, our results illustrate that Purkinje cells in SCA6 mice have an impaired ability to degrade other endocytosed cargo beyond BDNF and TrkB. This likely arises from trafficking deficits that result in a disruption in the transport of cargo to the lysosomes, along with lysosomal dysfunction.

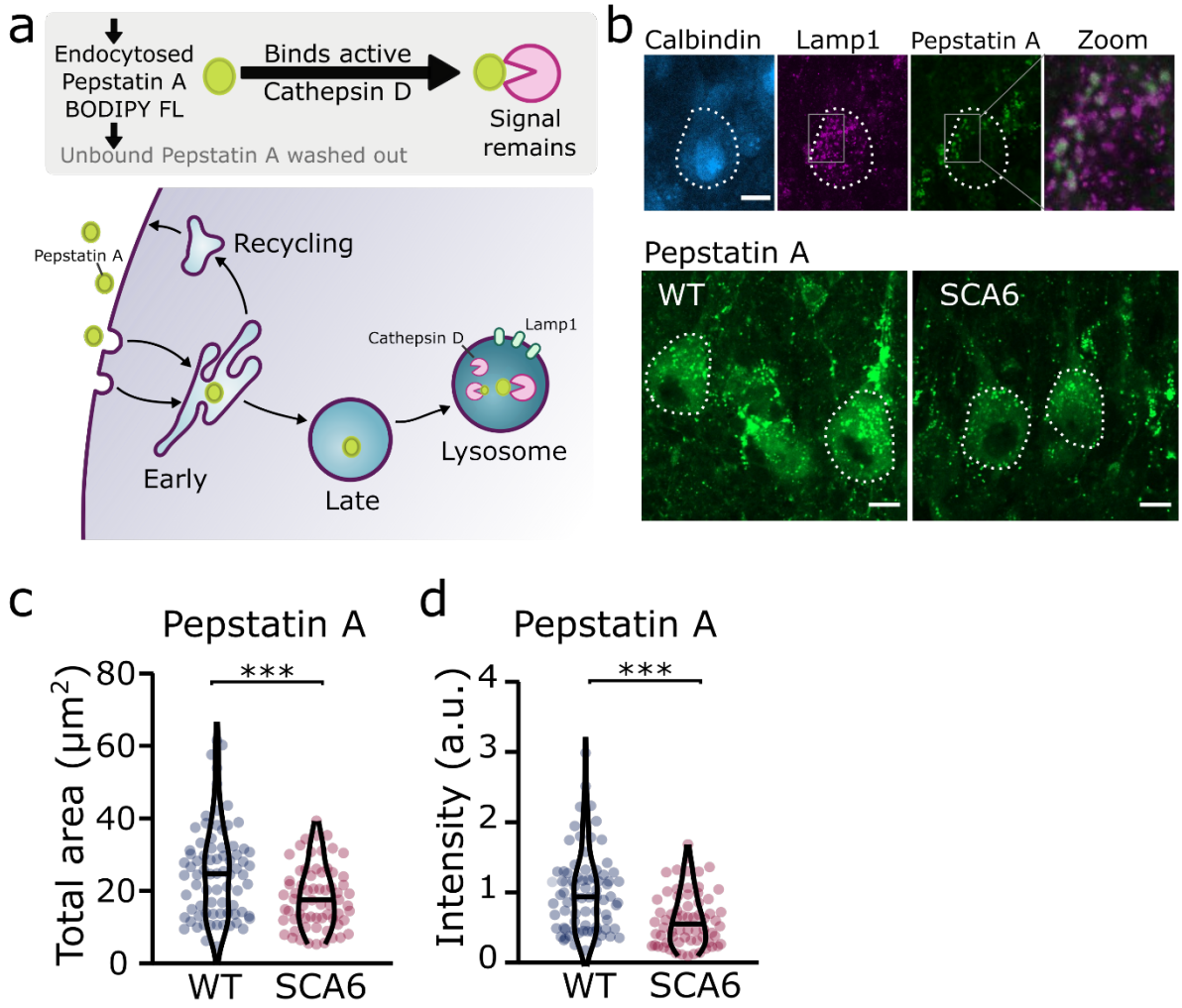

Figure 6: Trafficking of an exogenous peptide to the lysosome shows impairment in lysosomal action on endocytosed cargo in SCA6.
(a) Schematic showing the use of Pepstatin A BODIPY FL construct to visualize endosome trafficking and Cathepsin D activity. (b) Representative images of Pepstatin A staining in the anterior vermis. Top row shows colocalization with lysosome marker Lamp1, Calbindin labels Purkinje cells (outlined). Scale bars, 10μm (c) The area covered by Pepstatin A staining in Purkinje cells was significantly decreased in SCA6 mice ($P = 0.00076$; N = 3 WT mice, 78 cells; 3 SCA6 mice, 66 cells). (d) The intensity of Pepstatin A staining within Purkinje cells was significantly decreased in SCA6 mice ($P < 0.0001$; N = 3 WT mice, 78 cells; 3 SCA6 mice, 66 cells). Mann Whitney *U* test used for all statistical comparisons, *** $P < 0.001$.

TrkB activation with 7,8-DHF rescues deficits in early endosomes

We have previously shown that the TrkB agonist 7,8-DHF rescues deficits in motor coordination and Purkinje cell firing in SCA6 mice (Fig. 7a) (Cook et al., 2022). One interpretation of this rescue is that the TrkB agonist compensates for reduced levels of BDNF in the SCA6 cerebellum, thereby activating downstream signaling cascades to restore cerebellar function. However, we have also previously shown that TrkB activation with 7,8-DHF led to increased levels of TrkB in the SCA6 cerebellum (Cook et al., 2022), suggesting a role of autocrine signaling in the rescue, as TrkB activation appears to regulate its own

expression. Given that TrkB signaling is known to be involved in the regulation and trafficking of endosomes (Scott-Solomon and Kuruvilla, 2018), we wondered whether chronic oral administration of 7,8-DHF to SCA6 mice would rescue the deficits in early endosome size. We used the same treatment regimen of 7,8-DHF that had previously been shown to rescue deficits in behaviour and Purkinje cell firing, which comprised of 1 month of oral administration of the drug to peri-onset (6–7-month-old) SCA6 mice (Fig 7a). Half of the mice received control solution with no drug added. After one month of 7,8-DHF administration, cerebellar vermis sections were stained for BDNF and EEA1 as an early endosome marker, as previously described (Fig. 2). 7,8-DHF administration rescued the size of the early endosomes, with the total EEA1 area within Purkinje cells reducing to the WT level previously described (Fig. 7b, c). The level of BDNF accumulation within the early endosomes was also restored (Fig. 7d), suggesting that in addition to autocrine upregulation of TrkB (Cook et al., 2022), TrkB activation can normalize intracellular localization and trafficking of its endogenous ligand, consistent with its role in regulating endosome trafficking and function (Scott-Solomon and Kuruvilla, 2018).

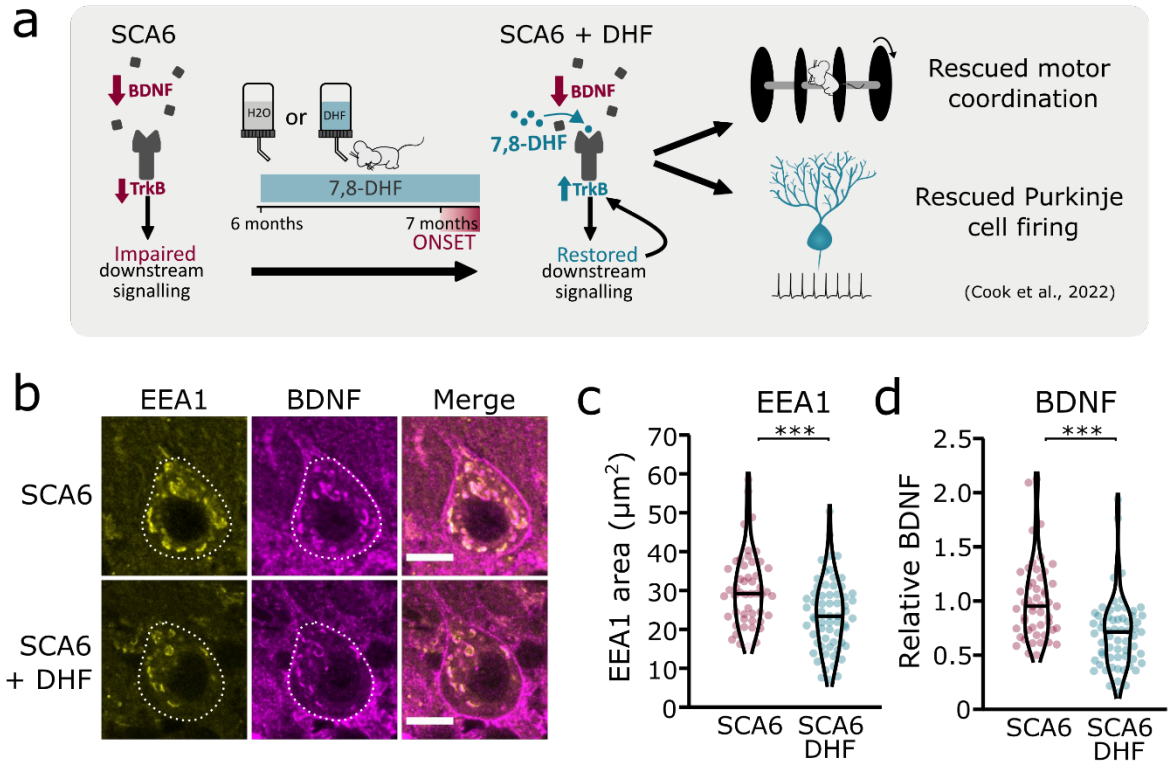

Figure 7: TrkB activation with 7,8-DHF rescues early endosomes deficits in SCA6 Purkinje cells. (a) Schematic showing 7,8-DHF administration to SCA6 mice and the previously described therapeutic benefits of 7,8-DHF in SCA6 mice. (b) Representative images of the early endosome marker EEA1 and BDNF within Purkinje cells (outlined) of the anterior vermis. Scale bar, 10μm. (c) The area covered by EEA1 staining in Purkinje cells is decreased in SCA6 mice given DHF compared to those that received control water ($P < 0.001$; Student's *t* test; N = 3 SCA6 mice, 50 cells; 3 SCA6 DHF mice, 63 cells). (d) Relative staining level of BDNF within early endosome compartment is decreased in the Purkinje cells of SCA6 mice that received DHF compared to controls ($P < 0.001$; Mann Whitney *U* test; N = 3 SCA6 mice, 50 cells; 3 SCA6 DHF mice, 63 cells). *** $P < 0.001$.

Discussion

We have identified multiple novel deficits in the endo-lysosomal pathway that could contribute to BDNF-TrkB signaling alterations in SCA6 (Fig. 8). Early endosomes were enlarged in SCA6 and accumulate BDNF and TrkB. Recycling endosomes were morphologically normal but carried less TrkB, and late endosomes were reduced in size and carried less BDNF. This suggests that cargo is getting stuck in the enlarged early endosomes in SCA6. The involvement of lysosomal pathology in SCA6 is less clear. Lysosomes appear morphologically normal with normal pH, but RNA-sequencing revealed upregulation of lysosomal genes in SCA6. SCA6 Purkinje cells also showed a reduction in exogenous cargo binding to the lysosomal enzyme Cathepsin D, indicating either a deficit in lysosomal enzyme activity, defects in endocytosis and cargo trafficking to lysosomes, or both. Taken together, these deficits could lead to cellular dysfunction in SCA6. This work further highlights how BDNF and TrkB deficits manifest in SCA6, and the potential of targeting this pathway therapeutically.

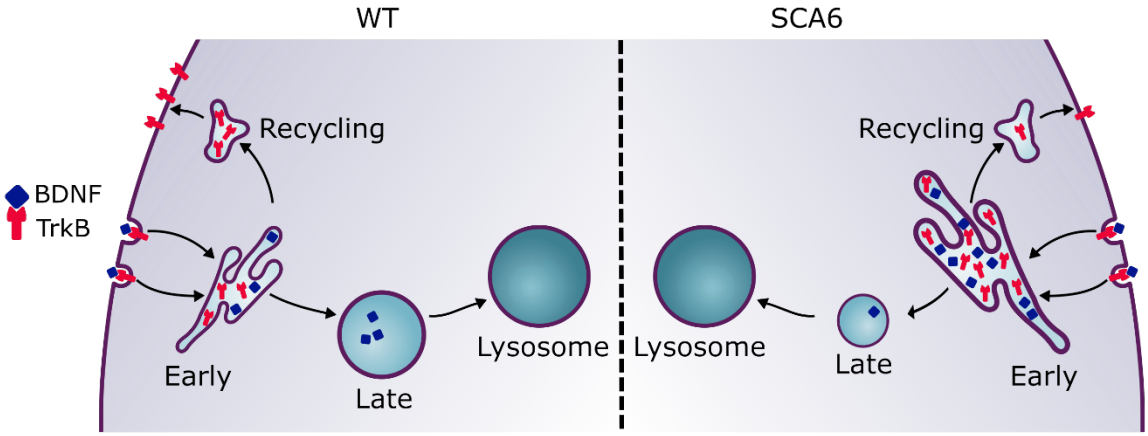

Figure 8: Multiple deficits in the endo-lysosomal system lead to abnormal localization of BDNF and TrkB in the Purkinje cells of SCA6 mice.

Excitingly, both the enlargement of early endosomes and the accumulation of BDNF in early endosomes could be rescued by the TrkB agonist, 7,8-DHF. There is evidence that TrkB can regulate its own expression and signaling (Cheng et al., 2011; Haapasalo et al., 2002) and we had previously shown that TrkB activation with the agonist 7,8-DHF increased levels of TrkB in the cerebellum of SCA6 mice (Cook et al., 2022). This new finding demonstrates that not only does TrkB activation with 7,8-DHF regulate the expression of TrkB in the SCA6 cerebellum, but also the localization of its ligand within endosomal compartments. This provides insight into the mechanisms by which BDNF and TrkB are regulated in the cerebellum. Furthermore, the finding that 7,8-DHF can rescue endosomal deficits in SCA6 supports the promise of 7,8-DHF and other TrkB agonists as potential treatments for SCA6 and raises the possibility of their use for treatment of other disorders displaying early endosome deficits.

This is important as early endosome deficits are not unique to SCA6. Enlargement of early endosomes is a hallmark of dysfunction in the endosomal pathway (Kaur and Lakkaraju, 2018) and has been observed in multiple diseases including Alzheimer's disease (Cataldo et al., 2004, 2000, 1997; Tate and Mathews, 2006), Down syndrome (Cataldo et al., 2000), models of macular degeneration (Kaur et al., 2018), Charcot-Marie-Tooth (Bucci et al., 2012) and Parkinson's disease (Vidyadhara et al., 2019). Early endosome abnormalities can arise from deficits in maturation or fusion of early endosomes, or alterations in the microtubule networks that govern endosome fusion (Skjeldal et al., 2012). Purkinje cells may be

382 particularly susceptible to early endosome enlargement, as in postmortem tissue from Niemann Pick type
383 C patients, Purkinje cells had enlarged early endosomes which accumulated amyloid precursor protein,
384 whereas in the hippocampus, pathology mostly concerned late endosomes (Jin et al., 2004). However,
385 endosomal pathology in SCA6 and other diseases is not limited to early endosomes, and other endosomal
386 compartments can be targeted therapeutically (Bonam et al., 2019; Tate and Mathews, 2006). In addition
387 to identifying TrkB activation as a therapeutic strategy for endosome deficits, our work opens the door for
388 the development of additional endosome-targeting treatment strategies for SCA6.
389
390 Our findings provide the first evidence for endosomal dysfunction contributing to signaling deficits in
391 spinocerebellar ataxias. Other ataxias like SCA1 also have reduced BDNF protein levels (Mellesmoen et
392 al., 2019), so it would be interesting to determine whether early endosome deficits could contribute to
393 disrupted BDNF signaling in other ataxias. Polyglutamine diseases in general are thought to have disruption
394 in protein degradation pathways (Chai et al., 1999; Cortes and La Spada, 2015), and SCA7 patients and
395 mouse models display alterations in lysosome pathways (Alves et al., 2014). Therefore, similar
396 abnormalities could be a common feature of similar diseases.
397
398 There remain, however, some unanswered questions from our study. What is the specific deficit that leads
399 to early endosome enlargement and other deficits? Is it the same as in other neurological diseases? Future
400 work to identify this will further aid in the development of endosome-targeting therapies. There is also the
401 question of the effect on other cargo. Sorting and recycling happens in a cargo-specific manner (Hu et al.,
402 2015) and so other cargo could be handled differently. Here we investigated endosomal trafficking of
403 BDNF and TrkB as we have previously shown this pathway to be both dysregulated in SCA6, and amenable
404 to therapeutic targeting. However, our experiments with BODIPY FL Pepstatin A suggest that even
405 exogenous cargo could be transported differently in SCA6. Future research should consider whether other
406 cargo accumulate in early endosomes and how this affects cell physiology. Furthermore, in parallel to
407 endocytosis and endosome trafficking, cells transport proteins for degradation in lysosomes via autophagy
408 (Klionsky, 2005). There are therefore two pathways with a common destination of degradation in
409 lysosomes, both of which are important for cell function, and abnormalities in one pathway can lead to
410 disruption in the other (Birgisdottir and Johansen, 2020; Mahapatra et al., 2019). Future work should
411 therefore investigate whether autophagy is disrupted in SCA6.

412 In summary, we have identified a dysregulated cellular trafficking pathway that contributes to cerebellar
413 pathophysiology that is novel not just in SCA6, but in SCAs in general. We found that several components
414 of the endo-lysosomal system show abnormalities in Purkinje cells in SCA6 mice. These deficits could
415 contribute to BDNF-TrkB signaling deficits in SCA6, as BDNF and TrkB accumulate in early endosomes
416 and there is a reduction in TrkB being recycled to the cell membrane for further signal transduction. The
417 endo-lysosomal system is therefore a promising therapeutic target for SCA6.
418
419
420
421
422
423
424
425
426
427
428

429 ## Methods

430 ### Animals

431 As previously described, the SCA6$^{84Q/84Q}$ mouse model is a knock-in mouse with a humanized 84 CAG
432 repeat expansion mutation at the *CACNA1A* locus (Jayabal et al., 2015; Watase et al., 2008). We bred
433 heterozygous mice to generate SCA6$^{84Q/84Q}$ and litter-matched WT control mice. Breeding mice were
434 originally purchased from Jackson laboratories (Bar Harbor, Maine; strain: B6.129S7-Cacna1atm3Hzo/J;
435 stock number: 008683) and primer sequences for genotyping were provided by Jackson laboratories. This
436 breeding setup allowed us to use experimental cohorts that contained litter- and sex-matched mice randomly
437 assigned to experimental groups. Both male and female mice were included in all experiments, and we did
438 not exclude any experimental animals from analysis. The only experiment that included pre-selection of
439 mice was for RNA Sequencing where mice were selected for tissue collection based on rotarod
440 performance, to include animals that were representative of their genotype. For all other experiments mice
441 were selected at random and none were excluded. Animal husbandry and procedures were approved by the
442 McGill Animal Care Committee in accordance with the Canadian Council on Animal Care guidelines. All
443 staining experiments were carried out on tissue from mice aged 7-8 months of age, except the Lamp1 and
444 Lysotracker staining which was carried out at 12 months of age.
445

446 ### RNA extraction and sequencing

447 RNA extraction was performed on tissues from 5 WT (2 male, 3 female) and 5 SCA6 (3 male, 2 female)
448 mice at 12 months of age. Experimental mice were selected based on rotarod performance in order to
449 identify mice that were phenotypically representative of their genotype. The experimental area and tools
450 were cleaned with RNAseZap (Sigma #R2020) to remove RNAse contamination prior to starting
451 experiments. Mice were anesthetised with isoflurane until the loss of toe pinch reflex, decapitated and the
452 cerebellar vermis was dissected, separated into anterior and posterior sections, flash frozen on dry ice, and
453 stored at -80°C until RNA extraction. RNA extraction proceeded as follows, with all procedures carried out
454 on ice or at 4°C. Cerebellar vermis tissue sections were mechanically homogenized in TRIzol reagent
455 (Invitrogen #15596026) by passing the lysate repeatedly through a series of needles, starting at 18-gauge,
456 followed by 23-gauge. Chloroform (Sigma #288306) was added to the homogenate to separate total RNA
457 in the aqueous phase, and RNA was recovered by precipitation with ethanol (70%). RNA extracts were
458 purified using the RNeasy Mini Kit (Qiagen #74104) with DNase I treatment as described in the
459 manufacturer's protocol.
460

461 The RNA integrity of samples was quantified with capillary electrophoresis (Agilent BioAnalyzer 2100) in
462 order to generate an RNA integrity number (RIN). All samples had an RIN over 7.5 and therefore were
463 assessed to have high RNA quality. Library preparation and sequencing was carried out by Genome Quebec
464 (Montreal, Quebec, Canada) using NEB stranded mRNA library prep, sequenced on the Illumina NovaSeq
465 6000 S4 generating 100bp paired-end reads. Samples had a median of 53 million reads (IQR, 42-64 million
466 reads), and a median of 92% mapping rate (IQR, 92%-92%).
467

468 ### RNA sequencing data analysis

469 The generated FASTQ files were transferred to the Digital Research Alliance of Canada cloud server for
470 processing and analysis. First, reads were aligned to the mouse reference genome (GRCm38) using HISAT2
471 version 2.1.0 (Kim et al., 2019). Quantification of reads was carried out with HTSeq version 0.11. (Anders
472 et al., 2015) in union mode. Reads generated from anterior and posterior samples were combined by
473 addition at this step to generate an *in silico* whole cerebellar vermis read count. Differential expression
474 analysis was performed with DESeq2 version 1.24.0 in RStudio (Love et al., 2014). DESeq2 adjusted P
475 values for multiple testing with a target $\alpha = 0.05$, and genes were considered to be differentially expressed

genes (DEGs) at FDR < 0.05. Enriched gene pathways were identified using gProfiler (Raudvere et al., 2019) based on terms in gene ontology (GO) databases.

Immunohistochemistry

Tissue sections for immunohistochemistry (IHC) were prepared as described previously (Cook et al., 2022). Mice were deeply anesthetised with 400mg/kg 2,2,2-tribromoethanol (Avertin) prepared in sterile 0.85% saline for a working concentration of 20mg/ml. Intracardiac perfusion comprised of a flush with 40mL of heparin in phosphate-buffered saline (PBS; 0.1 M, pH 7) followed by 40mL of 4% paraformaldehyde in phosphate buffer (PB). Brains were rapidly removed and incubated in 4% PFA for a further 24 hours of fixation at 4°C on an orbital shaker at 70RPM. Brains were dissected to separate the cerebellum and sliced using a vibrating microtome (5100mz Vibrotome, Campden Instruments, Loughborough, UK) into sections of 75 or 100µm thickness. Slices were kept at 4°C in PBS with 0.05% sodium azide to inhibit microbial growth before staining.

Free-floating slices were rinsed with PBS and incubated in primary antibody (Supplementary Table 2) and blocking solution with BSA for 3 days, then rinsed in PBS and incubated for 90 minutes with secondary antibodies (Supplementary Table 2). For experiments involving anti-mouse secondary antibodies, an additional incubation with Fab fragments (AffiniPure Fab Fragment Anti-Mouse IgG, Jackson Immunoresearch 715-007-003) was added prior to secondary antibody incubation. After a final PBS wash, stained slices were mounted using ProLong Gold Antifade mounting medium (Thermo Fisher Scientific, Waltham, USA) and stored at 4°C and protected from light prior to imaging.

For BDNF and TrkB staining, cerebellar slices were pre-treated with a heat-induced epitope retrieval step involving heating the slices in PBS to 95°C for ten minutes immediately prior to staining. Slices were allowed to cool and IHC procedures were carried out as normal.

Purkinje cells sometimes contained auto-fluorescent granules that were visible under excitation from a 561nm or 488 nm laser even without primary antibody incubation (Supp. Fig. 3). In order to ascertain that these granules were not interfering with the identification of endosomes or lysosomes, staining batches included a negative control slice from each animal where applicable. These slices underwent all of the usual blocking steps except primary antibodies were not added, while secondary antibody incubation and mounting proceeded as usual. In the case of the Pepstatin A negative controls, slices were incubated in ACSF without Pepstatin A BODIPY FL, and all other steps proceeded as usual. We found that although there was some background fluorescence signal in Purkinje and other cells, the intensity of the signal was lower than the staining from the antibodies of interest and was unlikely to interfere significantly with image analysis. This can be seen in side-by-side comparisons of raw images from the same mice in Supplementary figure 3.

Lysotracker

Lysotracker staining was carried out on acute cerebellar slices. Mice were anesthetised with isoflurane until the loss of toe pinch reflex and then were decapitated into ice cold artificial cerebrospinal fluid (ACSF: 125 mM NaCl, 2.5 mM KCl, 2 mM CaCl2, 1 mM MgCl2, 1.25 mM NaH2PO4, 26 mM NaHCO3, and 20 mM glucose, bubbled with 95% O2 and 5% CO2 (carbogen) to maintain pH at 7.3; osmolality ~316 mOsm). The brain was removed and dissected, and the cerebellar vermis was sectioned into 150µm sagittal slices using a VT 1200S vibratome (Leica Microsystems, Wetzlar, Germany) in ice cold ACSF. Slices were transferred to a slice chamber filled with 37°C ACSF bubbled with carbogen for 40 minutes before staining. Slices were then incubated in LysoTracker™ Red DND-99 (ThermoFisher L7528) that was dissolved in

523 room temperature ACSF at a concentration of 1:3000. Incubation occurred at room temperature on an
524 orbital shaker at 70RPM. After 5 minutes of incubation the slices were transferred to 4% PFA in PB for
525 post-fixation at 70RPM for one hour. Slices were then washed in PBS and prepared for
526 immunohistochemistry as outlined above.
527
528 **Pepstatin A**
529 Pepstatin A imaging was carried out on acute cerebellar slices prepared in the same way as for the
530 Lysotracker imaging outlined above. After slices were kept in 37°C ACSF bubbled with carbogen for 40
531 minutes they were incubated in Pepstatin A fl BODIPY (Thermofisher P12271) that was prepared at a
532 concentration of 1µg/ mL in room temperature ACSF. A stock solution of 1µg/ 1µl pepstatin A in DMSO
533 was prepared, to improve solubility, giving a final concentration of 0.001% DMSO in the incubation
534 solution. Incubation lasted 30 minutes at room temperature on an orbital shaker at 70 RPM. Slices were
535 then rinsed twice with PBS and transferred to 4% PFA for post-fixation at 70RPM for 30 minutes. Slices
536 either underwent further staining with immunohistochemistry for Lamp1 and calbindin or were mounted
537 onto slides immediately using ProLong Gold Antifade mounting medium (Thermo Fisher Scientific,
538 Waltham, USA) and stored at 4°C and protected from light.
539
540 **Image acquisition**
541 Imaging was performed using an LSM800 confocal microscope (Zeiss) equipped with Zen Blue software.
542 Images were acquired using 63x and 40x objectives at 1024 x 1024-pixel resolution. Imaging was carried
543 out by an experimenter who was blinded to the experimental condition of the slides. All imaging and
544 analysis was carried out in lobule 3 of the anterior vermis, a region of the cerebellum that we have
545 previously shown to display cellular deficits in SCA6 (Cook et al., 2022; Jayabal et al., 2015).
546
547 **Image Analysis**
548 Image analysis was performed in FIJI (ImageJ; US National Institutes of Health) (Rueden et al., 2017;
549 Schindelin et al., 2012). Purkinje cell bodies were delineated by hand using calbindin or BDNF as a marker
550 so that the Purkinje cell soma area could be isolated for further analysis. To calculate the area of the
551 endosomes or lysosomes, an Otsu thresholding function of the endosomal marker was used. Despeckle and
552 watershed functions were applied to create a region of interest consisting of the relevant endosomal
553 compartment within the cell. This was subsequently used as a mask to measure fluorescence intensity levels
554 of the cargo of interest. The cargo level was calculated using the integrated density measurement in ImageJ
555 within the region of interest delineating the compartment of interest, and all values were normalized to the
556 mean WT value. In figure 6 values were normalized to the mean SCA6 control value. Analysis was carried
557 out using custom ImageJ macros alongside manual verification.
558
559 For additional analysis of the lysosomes, we performed manual counts of Lamp1 and Lysotracker positive
560 organelles within individual Purkinje cells.
561
562 To improve the legibility of figure panels, linear adjustments of the brightness and contrast were applied to
563 some representative image sets. Adjustments were kept to a minimum and identical adjustments were
564 applied to images from all conditions, occurring after image analysis. Image analysis was performed on
565 raw images by an experimenter blinded to the experimental condition of the slides.
566
567 **7,8-DHF administration**
568 7,8-dihydroxyflavone (7,8-DHF) administration was carried out as previously described (Cook et al., 2022),
569 as we had previously found this treatment regimen to be both well tolerated and effective at restoring TrkB-

Akt signaling in SCA6 mice. Briefly, single-housed mice were provided with ad libitum access to drug solutions in place of their drinking water for 1 month. These solutions contained either 157.3 µM 7,8-DHF (TCI America) dissolved in 0.04% DMSO vehicle (Sigma, Oakville, ON, Canada) or 0.04% DMSO only as a control, dissolved in autoclaved water with 10% sucrose (Sigma, Oakville, ON, Canada) added to make the solutions palatable and disguise any taste of the drug. Solutions were prepared fresh at least twice weekly and replenished daily. It has been shown by us and others that oral administration of 7,8-DHF is sufficient to induce signaling changes in the brain (Cook et al., 2022; Gao et al., 2016; Johnson et al., 2012; Liu et al., 2016; Parrini et al., 2017; Zhang et al., 2013) and the drug has been shown to be orally bioavailable (Liu et al., 2013).

Statistical analysis

Pairwise statistical comparisons were carried out to identify statistical differences between groups. In cases where the data were normally distributed, Student's *t* tests were used, otherwise Mann Whitney *U* tests were used. The type of statistical test and the sample size is indicated in the figure legend for each plot. All violin plots show individual cells as data points, with the median displayed as a horizontal line.

Acknowledgements

We would like to thank all members of the Watt lab for helpful discussions and feedback on experiments, particularly to Kim Gruver for feedback on an earlier draft of this manuscript. Thank you to Anne McKinney, Louis-Charles Masson and Andy Gao for advice and guidance throughout the project. Thank you to Rose Bagot for technical advice regarding the RNA-Sequencing experiment.

We are grateful to Lois Lau and Anika Holur for carrying out genotyping and to Tanya Koch and all CMARC staff for animal colony support. Imaging was carried out in the McGill University Advanced BioImaging Facility (ABIF), RRID:SCR_017697 and we thank ABIF staff members for technical support. This research was enabled in part by support provided by Calcul Québec (calculquebec.ca) and the Digital Research Alliance of Canada (alliancecan.ca).

This work was funded by a CIHR project grant (PJT-153150) (AJW). Student support came from doctoral awards from the Fonds de recherche du Québec – Santé (AAC and TCSL), a MITACS training award (AAC), a McGill science undergraduate research award (MR), and a McGill Biology research award (ÉZD).

References

Akizu N, Cantagrel V, Zaki MS, Al-Gazali L, Wang X, Rosti RO, Dikoglu E, Gelot AB, Rosti B, Vaux KK, Scott EM, Silhavy JL, Schroth J, Copeland B, Schaffer AE, Gordts PLSM, Esko JD, Buschman MD, Field SJ, Napolitano G, Abdel-Salam GM, Ozgul RK, Saglroglu MS, Azam M, Ismail S, Aglan M, Selim L, Mahmoud IG, Abdel-Hadi S, Badawy A El, Sadek AA, Mojahedi F, Kayserili H, Masri A, Bastaki L, Temtamy S, Müller U, Desguerre I, Casanova JL, Dursun A, Gunel M, Gabriel SB, De Lonlay P, Gleeson JG. 2015. Biallelic mutations in SNX14 cause a syndromic form of cerebellar atrophy and lysosome-autophagosome dysfunction. *Nat Genet 2015 475* **47**:528–534. doi:10.1038/ng.3256

Alves S, Cormier-Dequaire F, Marinello M, Marais T, Muriel MP, Beaumatin F, Charbonnier-Beaupel F, Tahiri K, Seilhean D, El Hachimi K, Ruberg M, Stevanin G, Barkats M, den Dunnen W, Priault M, Brice A, Durr A, Corvol JC, Sittler A. 2014. The autophagy/lysosome pathway is impaired in SCA7 patients and SCA7 knock-in mice. *Acta Neuropathol* **128**:705–722. doi:10.1007/s00401-014-1289-8

618 Anders S, Pyl PT, Huber W. 2015. HTSeq—a Python framework to work with high-throughput
619 sequencing data. *Bioinformatics* **31**:166–169. doi:10.1093/BIOINFORMATICS/BTU638
620 Birgisdottir ÅB, Johansen T. 2020. Autophagy and endocytosis – interconnections and interdependencies.
621 *J Cell Sci* **133**. doi:10.1242/JCS.228114/224826
622 Bonam SR, Wang F, Muller S. 2019. Lysosomes as a therapeutic target. *Nat Rev Drug Discov 2019 1812*
623 **18**:923–948. doi:10.1038/s41573-019-0036-1
624 Bucci C, Bakke O, Progida C. 2012. Charcot–Marie–Tooth disease and intracellular traffic. *Prog*
625 *Neurobiol* **99**:191. doi:10.1016/J.PNEUROBIO.2012.03.003
626 Cataldo AM, Barnett JL, Pieroni C, Nixon RA. 1997. Increased Neuronal Endocytosis and Protease
627 Delivery to Early Endosomes in Sporadic Alzheimer's Disease: Neuropathologic Evidence for a
628 Mechanism of Increased β-Amyloidogenesis. *J Neurosci* **17**:6142–6151.
629 doi:10.1523/JNEUROSCI.17-16-06142.1997
630 Cataldo AM, Petanceska S, Terio NB, Peterhoff CM, Durham R, Mercken M, Mehta PD, Buxbaum J,
631 Haroutunian V, Nixon RA. 2004. Aβ localization in abnormal endosomes: association with earliest
632 Aβ elevations in AD and Down syndrome. *Neurobiol Aging* **25**:1263–1272.
633 doi:10.1016/J.NEUROBIOLAGING.2004.02.027
634 Cataldo AM, Peterhoff CM, Troncoso JC, Gomez-Isla T, Hyman BT, Nixon RA. 2000. Endocytic
635 pathway abnormalities precede amyloid β deposition in sporadic alzheimer's disease and down
636 syndrome: Differential effects of APOE genotype and presenilin mutations. *Am J Pathol* **157**:277–
637 286. doi:10.1016/S0002-9440(10)64538-5
638 Chai Y, Koppenhafer SL, Shoesmith SJ, Perez MK, Paulson HL. 1999. Evidence for Proteasome
639 Involvement in Polyglutamine Disease: Localization to Nuclear Inclusions in SCA3/MJD and
640 Suppression of Polyglutamine Aggregation in vitro. *Hum Mol Genet* **8**:673–682.
641 doi:10.1093/HMG/8.4.673
642 Chang HHV, Cook AA, Watt AJ, Cullen KE. 2022. Loss of Flocculus Purkinje Cell Firing Precision
643 Leads to Impaired Gaze Stabilization in a Mouse Model of Spinocerebellar Ataxia Type 6 (SCA6).
644 *Cells* **11**. doi:10.3390/cells11172739
645 Chazotte B. 2011. Labeling lysosomes in live cells with lysotracker. *Cold Spring Harb Protoc*
646 **6**:pdb.prot5571. doi:10.1101/pdb.prot5571
647 Chen CS, Chen WNU, Zhou M, Arttamangkul S, Haugland RP. 2000. Probing the cathepsin D using a
648 BODIPY FL-pepstatin A: Applications in fluorescence polarization and microscopy. *J Biochem*
649 *Biophys Methods* **42**:137–151. doi:10.1016/S0165-022X(00)00048-8
650 Cheng PL, Song AH, Wong YH, Wang S, Zhang X, Poo MM. 2011. Self-amplifying autocrine actions of
651 BDNF in axon development. *Proc Natl Acad Sci U S A* **108**:18430–18435.
652 Cheng XT, Xie YX, Zhou B, Huang N, Farfel-Becker T, Sheng ZH. 2018. Revisiting LAMP1 as a marker
653 for degradative autophagy-lysosomal organelles in the nervous system. *Autophagy*.
654 doi:10.1080/15548627.2018.1482147
655 Cook AA, Jayabal S, Sheng J, Fields E, Leung TCS, Quilez S, McNicholas E, Lau L, Huang S, Watt AJ.
656 2022. Activation of TrkB-Akt signaling rescues deficits in a mouse model of SCA6. *Sci Adv* **8**:3260.
657 doi:10.1126/sciadv.abh3260
658 Cortes CJ, La Spada AR. 2015. Autophagy in Polyglutamine Disease: Imposing Order on Disorder or
659 Contributing to the Chaos? *Mol Cell Neurosci* **66**:53. doi:10.1016/J.MCN.2015.03.010
660 de Duve C. 2005. The lysosome turns fifty. *Nat Cell Biol 2005 79* **7**:847–849. doi:10.1038/ncb0905-847
661 Du X, Wang J, Zhu H, Rinaldo L, Lamar K-M, Palmenberg AC, Hansel C, Gomez CM. 2013. Second
662 Cistron in CACNA1A Gene Encodes a Transcription Factor Mediating Cerebellar Development and
663 SCA6. *Cell* **154**:118–133. doi:10.1016/J.CELL.2013.05.059
664 Du X, Wei C, Hejazi Pastor DP, Rao ER, Li Y, Grasselli G, Godfrey J, Palmenberg AC, Andrade J,
665 Hansel C, Gomez CM. 2019. α1ACT Is Essential for Survival and Early Cerebellar Programming in
666 a Critical Neonatal Window. *Neuron*. doi:10.1016/J.NEURON.2019.02.036
667 Evans SF, Irmady K, Ostrow K, Kim T, Nykjaer A, Saftig P, Blobel C, Hempstead BL. 2011. Neuronal
668 Brain-derived Neurotrophic Factor Is Synthesized in Excess, with Levels Regulated by Sortilin-

669 mediated Trafficking and Lysosomal Degradation. *J Biol Chem* **286**:29556–29567.
670 doi:10.1074/JBC.M111.219675
671 Gao L, Tian M, Zhao HY, Xu QQ, Huang YM, Si QC, Tian Q, Wu QM, Hu XM, Sun LB, McClintock
672 SM, Zeng Y. 2016. TrkB activation by 7, 8-dihydroxyflavone increases synapse AMPA subunits
673 and ameliorates spatial memory deficits in a mouse model of Alzheimer's disease. *J Neurochem*
674 **136**:620–636. doi:10.1111/JNC.13432
675 Haapasalo A, Sipola I, Larsson K, Åkerman KEO, Stoilov P, Stamm S, Wong G, Castrén E. 2002.
676 Regulation of TRKB Surface Expression by Brain-derived Neurotrophic Factor and Truncated
677 TRKB Isoforms. *J Biol Chem* **277**:43160–43167. doi:10.1074/JBC.M205202200
678 Hu YB, Dammer EB, Ren RJ, Wang G. 2015. The endosomal-lysosomal system: From acidification and
679 cargo sorting to neurodegeneration. *Transl Neurodegener*. doi:10.1186/s40035-015-0041-1
680 Huotari J, Helenius A. 2011. Endosome maturation. *EMBO J*. doi:10.1038/emboj.2011.286
681 Jayabal S, Chang HHV, Cullen KE, Watt AJ. 2016. 4-aminopyridine reverses ataxia and cerebellar firing
682 deficiency in a mouse model of spinocerebellar ataxia type 6. *Sci Rep*. doi:10.1038/srep29489
683 Jayabal S, Ljungberg L, Erwes T, Cormier A, Quilez S, El Jaouhari S, Watt AJ. 2015. Rapid onset of
684 motor deficits in a mouse model of spinocerebellar ataxia type 6 precedes late cerebellar
685 degeneration. *eNeuro* **2**:ENEURO.0094-15.2015. doi:10.1523/ENEURO.0094-15.2015
686 Jin LW, Maezawa I, Vincent I, Bird T. 2004. Intracellular Accumulation of Amyloidogenic Fragments of
687 Amyloid-β Precursor Protein in Neurons with Niemann-Pick Type C Defects Is Associated with
688 Endosomal Abnormalities. *Am J Pathol* **164**:975–985. doi:10.1016/S0002-9440(10)63185-9
689 Johnson RA, Lam M, Punzo AM, Li H, Lin BR, Ye K, Mitchell GS, Chang Q. 2012. 7,8-
690 Dihydroxyflavone exhibits therapeutic efficacy in a mouse model of Rett syndrome. *J Appl Physiol*
691 **112**:704–710. doi:https://doi.org/10.1152/japplphysiol.01361.2011
692 Kaur G, Lakkaraju A. 2018. Early endosome morphology in health and diseaseAdvances in Experimental
693 Medicine and Biology. Springer New York LLC. pp. 335–343. doi:10.1007/978-3-319-75402-4_41
694 Kaur G, Tan LX, Rathnasamy G, Cunza N La, Germer CJ, Toops KA, Fernandes M, Blenkinsop TA,
695 Lakkaraju A. 2018. Aberrant early endosome biogenesis mediates complement activation in the
696 retinal pigment epithelium in models of macular degeneration. *Proc Natl Acad Sci U S A* **115**:9014–
697 9019. doi:10.1073/pnas.1805039115
698 Kim D, Paggi JM, Park C, Bennett C, Salzberg SL. 2019. Graph-based genome alignment and genotyping
699 with HISAT2 and HISAT-genotype. *Nat Biotechnol 2019 378* **37**:907–915. doi:10.1038/s41587-
700 019-0201-4
701 Kim S, Ochoa K, Melli SE, Yousufzai FAK, Barrera ZD, Williams AA, McIntyre G, Delgado E, Bolish
702 JN, Macleod CM, Boghos M, Lens HP, Ramos AG, Wilson VB, Maloney K, Padron ZM, Khan AH,
703 Blanco RE, Soto I. 2023. Disruptive lysosomal-metabolic signaling and neurodevelopmental deficits
704 that precede Purkinje cell loss in a mouse model of Niemann-Pick Type-C disease. *Sci Reports 2023*
705 *131* **13**:1–17. doi:10.1038/s41598-023-32971-0
706 Klionsky DJ. 2005. Autophagy. *Curr Biol* **15**:R282–R283. doi:10.1016/J.CUB.2005.04.013
707 Lawrence RE, Zoncu R. 2019. The lysosome as a cellular centre for signalling, metabolism and quality
708 control. *Nat Cell Biol 2019 212* **21**:133–142. doi:10.1038/s41556-018-0244-7
709 Liu C, Chan CB, Ye K. 2016. 7,8-dihydroxyflavone, a small molecular TrkB agonist, is useful for treating
710 various BDNF-implicated human disorders. *Transl Neurodegener* **5**:2. doi:10.1186/s40035-015-
711 0048-7
712 Liu X, Qi Q, Xiao G, Li J, Luo HR, Ye K. 2013. O-Methylated Metabolite of 7,8-Dihydroxyflavone
713 Activates TrkB Receptor and Displays Antidepressant Activity. *Pharmacology* **91**:185–200.
714 doi:10.1159/000346920
715 Love MI, Huber W, Anders S. 2014. Moderated estimation of fold change and dispersion for RNA-seq
716 data with DESeq2. *Genome Biol* **15**. doi:10.1186/S13059-014-0550-8
717 Ludwig T, Griffiths G, Hoflack B. 1991. Distribution of newly synthesized lysosomal enzymes in the
718 endocytic pathway of normal rat kidney cells. *J Cell Biol* **115**:1561–1572.
719 doi:10.1083/JCB.115.6.1561

720 Mahapatra KK, Panigrahi DP, Praharaj PP, Bhol CS, Patra S, Mishra SR, Behera BP, Bhutia SK. 2019.
721 Molecular interplay of autophagy and endocytosis in human health and diseases. *Biol Rev* **94**:1576–
722 1590. doi:10.1111/BRV.12515
723 Majzoub RN, Wonder E, Ewert KK, Kotamraju VR, Teesalu T, Safinya CR. 2016. Rab11 and
724 Lysotracker Markers Reveal Correlation between Endosomal Pathways and Transfection Efficiency
725 of Surface-Functionalized Cationic Liposome-DNA Nanoparticles. *J Phys Chem B* **120**:6439–6453.
726 doi:10.1021/acs.jpcb.6b04441
727 Mannan AU, Roussa E, Kraus C, Rickmann M, Maenner J, Nayernia K, Krieglstein K, Reis A, Engel W.
728 2004. Mutation in the gene encoding lysosomal acid phosphatase (Acp2) causes cerebellum and skin
729 malformation in mouse. *Neurogenetics* **5**:229–238. doi:10.1007/S10048-004-0197-9/FIGURES/6
730 Mellesmoen A, Sheeler C, Ferro A, Rainwater O, Cvetanovic M. 2019. Brain Derived Neurotrophic
731 Factor (BDNF) Delays Onset of Pathogenesis in Transgenic Mouse Model of Spinocerebellar
732 Ataxia Type 1 (SCA1). *Front Cell Neurosci* **12**:509. doi:10.3389/fncel.2018.00509
733 Moya-Alvarado G, Gonzalez A, Stuardo N, Bronfman FC. 2018. Brain-derived neurotrophic factor
734 (BDNF) regulates Rab5-positive early endosomes in hippocampal neurons to induce dendritic
735 branching. *Front Cell Neurosci* **12**. doi:10.3389/fncel.2018.00493
736 Moya-Alvarado G, Tiburcio-Felix R, Ibáñez MR, Aguirre-Soto AA, Guerra M V., Wu C, Mobley WC,
737 Perlson E, Bronfman FC. 2023. BDNF/TrkB signaling endosomes in axons coordinate
738 CREB/mTOR activation and protein synthesis in the cell body to induce dendritic growth in cortical
739 neurons. *Elife* **12**. doi:10.7554/eLife.77455
740 O'Sullivan MJ, Lindsay AJ. 2020. The endosomal recycling pathway—at the crossroads of the cell. *Int J*
741 *Mol Sci*. doi:10.3390/ijms21176074
742 Parrini M, Ghezzi D, Deidda G, Medrihan L, Castroflorio E, Alberti M, Baldelli P, Cancedda L,
743 Contestabile A. 2017. Aerobic exercise and a BDNF-mimetic therapy rescue learning and memory
744 in a mouse model of Down syndrome. *Sci Rep* **7**:16825. doi:10.1038/s41598-017-17201-8
745 Pescosolido MF, Ouyang Q, Liu JS, Morrow EM. 2021. Loss of Christianson Syndrome Na+/H+
746 Exchanger 6 (NHE6) Causes Abnormal Endosome Maturation and Trafficking Underlying
747 Lysosome Dysfunction in Neurons. *J Neurosci* **41**:9235–9256. doi:10.1523/JNEUROSCI.1244-
748 20.2021
749 Prekeris R, Klumperman J, Chen YA, Scheller RH. 1998. Syntaxin 13 mediates cycling of plasma
750 membrane proteins via tubulovesicular recycling endosomes. *J Cell Biol* **143**:957–971.
751 doi:10.1083/jcb.143.4.957
752 Raudvere U, Kolberg L, Kuzmin I, Arak T, Adler P, Peterson H, Vilo J. 2019. g:Profiler: a web server for
753 functional enrichment analysis and conversions of gene lists (2019 update). *Nucleic Acids Res*
754 **47**:W191–W198. doi:10.1093/NAR/GKZ369
755 Rueden CT, Schindelin J, Hiner MC, DeZonia BE, Walter AE, Arena ET, Eliceiri KW. 2017. ImageJ2:
756 ImageJ for the next generation of scientific image data. *BMC Bioinformatics* **18**:529.
757 doi:10.1186/s12859-017-1934-z
758 Schindelin J, Arganda-Carreras I, Frise E, Kaynig V, Longair M, Pietzsch T, Preibisch S, Rueden C,
759 Saalfeld S, Schmid B, Tinevez JY, White DJ, Hartenstein V, Eliceiri K, Tomancak P, Cardona A.
760 2012. Fiji: An open-source platform for biological-image analysis. *Nat Methods*.
761 doi:10.1038/nmeth.2019
762 Scott-Solomon E, Kuruvilla R. 2018. Mechanisms of Neurotrophin Trafficking via Trk Receptors. *Mol*
763 *Cell Neurosci* **91**:25. doi:10.1016/J.MCN.2018.03.013
764 Skjeldal FM, Strunze S, Bergeland T, Walseng E, Gregers TF, Bakke O. 2012. The fusion of early
765 endosomes induces molecularmotor- driven tubule formation and fission. *J Cell Sci* **125**:1910–1919.
766 doi:10.1242/jcs.092569
767 Solodkin A, Gomez CM. 2012. Spinocerebellar ataxia type 6. *Handb Clin Neurol* **103**:461–473.
768 doi:10.1016/B978-0-444-51892-7.00029-2
769 Song JW, Misgeld T, Kang H, Knecht S, Lu J, Cao Y, Cotman SL, Bishop DL, Lichtman JW. 2008.
770 Lysosomal Activity Associated with Developmental Axon Pruning. *J Neurosci* **28**:8993.

771 doi:10.1523/JNEUROSCI.0720-08.2008
772 Stenmark H. 2009. Rab GTPases as coordinators of vesicle traffic. *Nat Rev Mol Cell Biol 2009 108*
773 **10**:513–525. doi:10.1038/nrm2728
774 Sterling FR, D'Amico J, Brumfield AM, Huegel KL, Vaughan PS, Morris K, Schwarz S, Joyce M V.,
775 Boggess B, Champion MM, Maciuba K, Allen P, Marasco E, Koch G, Gonzalez P, Hodges S,
776 Leahy S, Gerstbauer E, Hinchcliffe EH, Vaughan KT. 2023. StARD9 is a novel lysosomal kinesin
777 required for membrane tubulation, cholesterol transport and Purkinje cell survival. *J Cell Sci* **136**.
778 doi:10.1242/JCS.260662/VIDEO-10
779 Tate BA, Mathews PM. 2006. Targeting the role of the endosome in the pathophysiology of Alzheimer's
780 disease: a strategy for treatment. *Sci Aging Knowledge Environ* **2006**.
781 doi:10.1126/SAGEKE.2006.10.RE2/ASSET/EA0BA019-D870-4C63-AD9F-
782 D51957355788/ASSETS/GRAPHIC/102006RE2F1.JPEG
783 Unno T, Wakamori M, Koike M, Uchiyama Y, Ishikawa K, Kubota H, Yoshida T, Sasakawa H, Peters C,
784 Mizusawa H, Watase K. 2012. Development of Purkinje cell degeneration in a knockin mouse
785 model reveals lysosomal involvement in the pathogenesis of SCA6. *Proc Natl Acad Sci U S A*
786 **109**:17693–8. doi:10.1073/pnas.1212786109
787 Vanier MT. 2010. Niemann-Pick disease type C. *Orphanet J Rare Dis*. doi:10.1186/1750-1172-5-16
788 Vidyadhara DJ, Lee JE, Chandra SS. 2019. Role of the Endolysosomal System in Parkinson's disease. *J*
789 *Neurochem* **150**:487. doi:10.1111/JNC.14820
790 Vitelli R, Santillo M, Lattero D, Chiariello M, Bifulco M, Bruni CB, Bucci C. 1997. Role of the small
791 GTPase RAB7 in the late endocytic pathway. *J Biol Chem* **272**:4391–4397.
792 doi:10.1074/jbc.272.7.4391
793 Watase K, Barrett CF, Miyazaki T, Ishiguro T, Ishikawa K, Hu Y, Unno T, Sun Y, Kasai S, Watanabe M,
794 Gomez CM, Mizusawa H, Tsien RW, Zoghbi HY. 2008. Spinocerebellar ataxia type 6 knockin mice
795 develop a progressive neuronal dysfunction with age-dependent accumulation of mutant CaV2.1
796 channels. *Proc Natl Acad Sci U S A* **105**:11987–92. doi:10.1073/pnas.0804350105
797 Yamashita N, Kuruvilla R. 2016. Neurotrophin signaling endosomes: Biogenesis, regulation, and
798 functions. *Curr Opin Neurobiol*. doi:10.1016/j.conb.2016.06.004
799 Zaidi N, Maurer A, Nieke S, Kalbacher H. 2008. Cathepsin D: A cellular roadmap. *Biochem Biophys Res*
800 *Commun*. doi:10.1016/j.bbrc.2008.08.099
801 Zhang Z, Liu X, Schroeder JP, Chan CB, Song M, Yu SP, Weinshenker D, Ye K. 2013. 7,8-
802 Dihydroxyflavone Prevents Synaptic Loss and Memory Deficits in a Mouse Model of Alzheimer's
803 Disease. *Neuropsychopharmacol 2014 393* **39**:638–650. doi:10.1038/npp.2013.243
804 Zhu F, Miao Y, Cheng M, Ye X, Chen A, Zheng G, Tian X. 2022. The CACNA1A Mutant Disrupts
805 Lysosome Calcium Homeostasis in Cerebellar Neurons and the Resulting Endo-Lysosomal Fusion
806 Defect Can be Improved by Calcium Modulation. *Neurochem Res* **47**:249–263. doi:10.1007/s11064-
807 021-03438-3
808 Zhuchenko O, Bailey J, Bonnen P, Ashizawa T, Stockton DW, Amos C, Dobyns WB, Subramony SH,
809 Zoghbi HY, Lee CC. 1997. Autosomal dominant cerebellar ataxia (SCA6) associated with small
810 polyglutamine expansions in the alpha 1A-voltage-dependent calcium channel. *Nat Genet* **15**:62–9.
811 doi:10.1038/ng0197-62
812